JOURNAL OF AIRCRAFT
Vol. 48, No. 2, March–April 2011

Elastic Deformation Analysis of Adhesively Bonded Composite Butt Joints in Tension

Gang Li,* Andrew Johnston,† Marko Yanishevsky,‡ and Nicholas C. Bellinger§
National Research Council Canada, Ottawa, Ontario, K1A 0R6 Canada

DOI: 10.2514/1.C031164

An elastic deformation analysis of bonded composite butt joints in tension was carried out. Theoretical expressions of the effective Young's modulus and bending stiffness for laminated composite beam panels were derived under both plane-strain and plane-stress conditions. Secondary bending deformation for bonded composite butt joints was analyzed theoretically. Joint elongation was estimated using a theoretical expression presented herein. An approach was proposed to eliminate the strain discontinuity at the joint overlap end, an artifact of inappropriate use of the Euler–Bernoulli beam theory. Expressions for the four coefficients arising from the coupled adhesive stress differential equations used were provided, and two strategies were proposed to explore the complete closed-form adhesive stress solutions in a general composite butt joint configuration. Two butt joint cases are presented. The case 1 joint was fabricated using identical laminated composite panels for both the adherends and the doubler, while the thickness of the doubler of the case 2 joint was 50% thicker. Three-dimensional finite element models were created for analysis of the unit-width joints under a plane-strain condition. Good agreement for the predicted joint deformation (deflection, elongation, and strain) was achieved between the three methods. Finite element results showed that high peak adhesive stresses were developed at the inner overlap edge area, and they suggested that appropriate reinforcement should be made in this region to ensure structural integrity.

Nomenclature

A_1, A_2, A_3	=	integration constants in the joint deflection expressions
a_1, a_2, b_1, b_2	=	four basic parameters in the adhesive stress differential equations
B_1, B_2, B_3	=	integration constants in the joint deflection expressions
E_a, G_a	=	adhesive Young's modulus and shear modulus
E_{xx}, D_x	=	effective Young's modulus and bending stiffness of laminates
k_{11}, k_{12}, k_{22}	=	elements in the compliance matrix of the in-plane constitutive relation for a classic Euler–Bernoulli composite beam, provided there are no transverse loads
L	=	outer unbonded adherend length
$[M], [N]$	=	unit-width moment and in-plane force matrices of laminated composites
T	=	unit-width joint remote tensile force, N/mm
t_1, t_2	=	thicknesses of adherend and doubler, respectively
Δl	=	joint elongation
η	=	adhesive layer thickness
μ_1, μ_2, μ_3	=	joint parameters
σ_a, τ_a	=	adhesive peel and shear stresses
$2c$	=	bondline length on one-sided overlap section between one adherend and doubler
$2L_0$	=	length of inner unbonded (or unoverlapped) doubler gap section

Presented as Paper 2010-3103 at the 51st AIAA/ASME/ASCE/AHS/ASC Structures, Structural Dynamics, and Materials Conference, Orlando, FL, 12–15 April 2010; received 24 June 2010; revision received 21 September 2010; accepted for publication 5 October 2010.

*Associate Research Officer, Structures and Materials Performance Laboratory, Institute for Aerospace Research, 1200 Montreal Road; Gang.Li@nrc-cnrc.gc.ca. Member AIAA (Corresponding Author).

†Group Leader, Senior Research Officer, Composites and Novel Airframe Materials, Structures and Materials Performance Laboratory, Institute for Aerospace Research, 1200 Montreal Road.

‡Senior Research Officer, Structures and Materials Performance Laboratory, Institute for Aerospace Research, 1200 Montreal Road.

§Group Leader, Principal Research Officer, Aerospace Structures, Structures and Materials Performance Laboratory, Institute for Aerospace Research, 1200 Montreal Road. Member AIAA.

I. Introduction

FIBER-REINFORCED composite primary and secondary aircraft structures have the potential to achieve the same strength and stiffness as conventional metallic structures but at substantially lower weight. Quasi-isotropic laminated composite panels are often used in aircraft applications [1–4], since these types of layups maintain satisfactory strength in both the longitudinal and hoop directions. A recent high-profile example of the rapid expansion of the use of composites in commercial aircraft is the Boeing 787, which includes composite fuselage barrel sections as large as 6 m in diameter and 15 m long.¶ This aircraft has its entire fuselage structure assembled by joining together several precured full-circumference barrel sections. To accomplish this in an efficient and cost-effective manner, the composite joints used to attach these structures are critical. One possible joint option for these types of structures is the single-strap butt joint configuration. With recent achievements in adhesive and bonding technologies, bonded joints can be both lighter and more cost effective than equivalent bolted or riveted joints. As such, joints with high-moduli high-strength adhesives have the potential to have much higher static strengths than bolted joints [4]. To supplement adhesive bonding, additional mechanical fasteners can be introduced to enhance structural integrity using a hybrid (bonded and bolted) attachment approach. To use this approach, understanding the deformation behavior of the bonded butt joints is essential. This is the subject of the current study.

The single-strap butt joint is actually fabricated by attaching two single-lap joints end to end [5–7]. In this configuration, the joint inner overlap edge will experience much greater bending moments than the outer overlap end when the joint is loaded in tension due to secondary bending [8].

¶Data available at http://www.boeing.com/news/releases/2005/q1/nr_050111g.html [retrieved 11 January 2005].

A recent survey of open literature on bonded composite joints [2,4,7–13] showed the following:

1) Limited experimental data on the butt joint configuration have been released publicly [13].

2) A theoretical analysis of laminated composite beams in bending has not been carried out simultaneously for both plane-strain and plane-stress conditions due to the lack of relevant well-defined parameters in effective Young's modulus and bending stiffness [8,9,14–17].

3) The difference between parameters, such as the effective Young's modulus, bending stiffness, and the obtained strains induced by these two conditions, has not been studied [8,9,14–16].

4) No papers were found that theoretically estimate the strain at the overlap end region in bonded joints.

In this paper, elastic deformation of an adhesively bonded composite single-strap butt joint configuration in tension was investigated, addressing the knowledge gaps identified in the literature survey. The completed theoretical explorations included 1) deriving expressions for the effective Young's modulus and bending deformation under both plane-strain and plane-stress conditions, 2) a study of the secondary bending deformation, 3) developing an expression to predict the joint elongation, 4) devising an approach to eliminate the strain discontinuity at the overlap end in the doubler, 5) providing expressions for the four coefficients in the coupled adhesive stress equations, and 6) suggesting two strategies to explore the complete closed-form adhesive stress solutions for bonded composite butt joints with different adherends and doublers.

Experimental tests on two different joint cases were carried out. The only feature that was different between the cases was the thickness of the doubler. The case 1 joint was fabricated using identical-thickness laminated composite panels for both the adherends and the doubler, while the doubler in the case 2 joint was 50% thicker than that used in the case 1 joint. The carbon-fiber laminates were laid up using an automated fiber placement (AFP) machine at the National Research Council Canada Institute for Aerospace Research, Aerospace Manufacturing Technology Centre, located in Montreal, Quebec. Joint dimensions were determined according to a previous study [8]. Joint elongation between the cross heads of a load frame was measured during loading, as were strains at key positions, using strain gauges. In addition, geometrically nonlinear finite element analyses (FEAs) were also carried out for a thorough study, with both experimental and theoretical methods.

The main objectives of the work presented in this paper were to 1) provide the necessary parameters for a relevant theoretical study on joint deformation and adhesive stress distribution, 2) support further theoretical evaluation of the impact of using plane-strain and/or plane-stress assumptions on the strain analysis, and 3) enrich the existing test data pool on bonded composite joint configurations, supporting improved design of composite joints.

II. Theoretical Preparations

Under most conditions, the composite adherend and doubler in a structure will behave in a linear elastic manner, while the adhesive may exhibit elastic as well as viscoelastic and/or nonlinear response. Fully capturing material nonlinearities would make an exact analytical treatment of the structural and material behaviors very complicated. Therefore, a linear elastic response of adherend, doubler, and adhesive was assumed in the theoretical analyses conducted here. Furthermore, a simplified joint configuration, without consideration of adhesive fillets, was used. Peak adhesive stress is usually located at the overlap end, with the greatest magnitude being at the butt joint inner edge [18]. Joint bending deformation and adhesive stress variations and magnitude are critical in the joint analysis. Good design can effectively reduce both the joint secondary bending and the adhesive stress magnitude, especially the adhesive peel stress. In this section, relevant theoretical preparations for analyzing the bonded butt laminated joint structures are presented and are then used to theoretically predict joint deformation and force (tension, shear, and bending) conditions at the overlap ends and to further identify the adhesive stresses. In this manner, better joint analysis could be achieved.

A. Theoretical Formulations for Laminated Composite Bending Analysis

For the classic Euler–Bernoulli beam, with no transverse loads, the in-plane constitutive relationship can be simplified from the constitutive equation for anisotropic composite laminates [14] by keeping only relevant strains and forces, as

$$\begin{bmatrix} \varepsilon_x^0 \\ \kappa_x \end{bmatrix} = \begin{bmatrix} k_{11} & k_{12} \\ k_{12} & k_{22} \end{bmatrix} \begin{bmatrix} N_x \\ M_x \end{bmatrix} \tag{1a}$$

where k_{11}, k_{12}, and k_{22} are compliance elements. They can be identified under both plane-strain (cylindrical bending) and plane-stress (classic beam) conditions. For symmetric and balanced laminates, the term k_{12} is zero. The effective or equivalent Young's modulus E_{xx} and bending stiffness D_x of the laminate can then be expressed as

$$E_{xx} = \frac{1}{tk_{11}} \tag{1b}$$

$$D_x = (EI)_{xx} = \frac{1}{k_{22}} \tag{1c}$$

where t is the laminate thickness.

1. *Plane-Strain Condition: Cylindrical Bending Laminates*

The plane-strain condition refers to a cylindrical bending laminate condition. In this case, the laminate is assumed to have infinite length along its width (y direction) and to be uniformly supported along its edges at $x = 0$ and l. The deformation of the laminate is then a function of x, with the terms ε_y^0, κ_y, and κ_{xy} equal to zero. Thus, the in-plane midplane strain and curvature can be determined as [14]

$$\begin{bmatrix} \varepsilon_x^0 \\ \gamma_{xy}^0 \\ \kappa_x \end{bmatrix} = \begin{bmatrix} A_{11} & A_{16} & B_{11} \\ A_{16} & A_{66} & B_{16} \\ B_{11} & B_{16} & D_{11} \end{bmatrix}^{-1} \begin{bmatrix} N_x \\ N_{xy} \\ M_x \end{bmatrix} \tag{2a}$$

where A_{ij}, B_{ij}, and D_{ij} are elements in the stiffness (**ABD**) matrix of the laminate constitutive equation; N_x, N_{xy}, and M_x are unit-width in-plane forces and moments.

The in-plane shear force N_{xy} is equal to zero in this bending situation; hence, Eq. (2a) becomes

$$\begin{bmatrix} \varepsilon_x^0 \\ \kappa_x \end{bmatrix} = \frac{\begin{bmatrix} A_{66}D_{11} - B_{16}^2 & A_{16}B_{16} - A_{66}B_{11} \\ A_{16}B_{16} - A_{66}B_{11} & A_{11}A_{66} - A_{16}^2 \end{bmatrix} \begin{bmatrix} N_x \\ M_x \end{bmatrix}}{A_{11}(A_{66}D_{11} - B_{16}^2) + 2A_{16}B_{11}B_{16} - D_{11}A_{16}^2 - A_{66}B_{11}^2} \tag{2b}$$

The effective Young's modulus and bending stiffness can be expressed as

$$E_{xx} = \frac{1}{t(A_{66}D_{11} - B_{16}^2)}[A_{11}(A_{66}D_{11} - B_{16}^2) + 2A_{16}B_{11}B_{16} - D_{11}A_{16}^2 - A_{66}B_{11}^2] \tag{2c}$$

$$D_x = (EI)_{xx} = \frac{1}{(A_{11}A_{66} - A_{16}^2)}[D_{11}(A_{11}A_{66} - A_{16}^2) + 2A_{16}B_{11}B_{16} - A_{11}B_{16}^2 - A_{66}B_{11}^2] \tag{2d}$$

The bending stiffness is the same as that developed by Whitney [14]. When the laminate is symmetrical and balanced, $B_{ij} = 0$ and $A_{16} = A_{26} = 0$. Therefore,

$$\begin{bmatrix} \varepsilon_x^0 \\ \kappa_x \end{bmatrix} = \begin{bmatrix} k_{11} & k_{12} \\ k_{12} & k_{22} \end{bmatrix} \begin{bmatrix} N_x \\ M_x \end{bmatrix} = \begin{bmatrix} \frac{1}{A_{11}} & 0 \\ 0 & \frac{1}{D_{11}} \end{bmatrix} \begin{bmatrix} N_x \\ M_x \end{bmatrix} \tag{2e}$$

The effective parameters, E_{xx} and D_x, can be further simplified as

$$E_{xx} = \frac{1}{tk_{11}} = \frac{A_{11}}{t} \tag{2f}$$

$$D_x = (EI)_{xx} = \frac{M_x}{\kappa_x} = D_{11} \tag{2g}$$

The same parameters in Eqs. (2f) and (2g) were used by Fridman and Abramovich [15].

2. Plane-Stress Condition: Classic Beam Theory

To employ the Euler–Bernoulli beam theory, a laminate must be symmetrical and balanced, such that $B_{ij} = 0$ and $A_{16} = A_{26} = 0$. Generally, coupling cannot be completely eliminated in laminates [14]; for instance, the terms D_{16} and D_{26} in the stiffness **ABD** matrix are usually not zero in symmetrical and balanced laminates, thus bending–twisting coupling still exists. For symmetrical and balanced laminates, the midplane strains and curvatures can be determined as [14]

$$\begin{bmatrix} \varepsilon_x^0 \\ \varepsilon_y^0 \\ \gamma_{xy}^0 \end{bmatrix} = \begin{bmatrix} A_{11} & A_{12} & 0 \\ A_{12} & A_{22} & 0 \\ 0 & 0 & A_{66} \end{bmatrix}^{-1} \begin{bmatrix} N_x \\ N_y \\ N_{xy} \end{bmatrix} \tag{3a}$$

$$\begin{bmatrix} \kappa_x \\ \kappa_y \\ \kappa_{xy} \end{bmatrix} = \begin{bmatrix} D_{11} & D_{12} & D_{16} \\ D_{12} & D_{22} & D_{26} \\ D_{16} & D_{26} & D_{66} \end{bmatrix}^{-1} \begin{bmatrix} M_x \\ M_y \\ M_{xy} \end{bmatrix} \tag{3b}$$

For laminated composite beams, it can be assumed that deflection is a function of x only, both in-plane forces (N_y and N_{xy}) are zero, and moments (M_y and M_{xy}) are small enough to be neglected [16]. As a result, the following simplified relationship can be established:

$$\begin{bmatrix} \varepsilon_x^0 \\ \kappa_x \end{bmatrix} = \begin{bmatrix} k_{11} & k_{12} \\ k_{12} & k_{22} \end{bmatrix} \begin{bmatrix} N_x \\ M_x \end{bmatrix} = \begin{bmatrix} k_{11} & 0 \\ 0 & k_{22} \end{bmatrix} \begin{bmatrix} N_x \\ M_x \end{bmatrix} \tag{3c}$$

By comparing the corresponding terms in Eqs. (3a–3c), the value of k_{11} and k_{22} can be identified as

$$k_{11} = \frac{A_{22}A_{66}}{A_{11}A_{22}A_{66} - A_{12}^2 A_{66}} \tag{3d}$$

$$k_{22} = \frac{D_{22}D_{66} - D_{26}^2}{D_{11}D_{22}D_{66} + 2D_{12}D_{16}D_{26} - D_{22}D_{16}^2 - D_{11}D_{26}^2 - D_{66}D_{12}^2} \tag{3e}$$

The effective parameters, E_{xx} and D_x, are thus

$$E_{xx} = \frac{1}{tk_{11}} = \frac{1}{t}\left(A_{11} - \frac{A_{12}^2}{A_{22}}\right) \tag{3f}$$

$$D_x = \frac{1}{k_{22}} = D_{11} - \frac{D_{22}D_{16}^2 + D_{66}D_{12}^2 - 2D_{12}D_{16}D_{26}}{D_{22}D_{66} - D_{26}^2} \tag{3g}$$

The preceding expression for the bending stiffness can also be derived from the work of Whitney [14]. Since the terms D_{16} and D_{26} in Eq. (3g) are small and can be neglected, the expression for bending stiffness can be simplified as

$$D_x = (EI)_{xx} = D_{11} - D_{12}^2/D_{22} \tag{3h}$$

The same effective Young's modulus and bending stiffness were used by Machado [17].

B. Bonded Single-Strap Butt Composite Joint in Tension

The Euler–Bernoulli beam theory can be used to determine the elastic secondary bending deformation of the composite joints when these joints are loaded in tension. Bending deformation for practical aircraft joint structures should be studied using the plane-strain condition due to the large joint width and a firmly constrained displacement condition. However, the bending response of joint coupons, with a finite width, lies between the two idealized conditions (i.e., the plane strain and plane stress). Thus, calculations under both plane-strain and plane-stress conditions should be carried out to determine upper and lower bounds for the joint coupon deformation.

1. Deflection and Bending Moment

Theoretical analysis of joints is usually carried out using a simplified configuration without adhesive fillets at the overlap ends. Joint bending can be analyzed using beam theory, as initially suggested by Goland and Reissner in 1944 [5]. As shown in Fig. 1, a butt joint has three sections: an outer unbonded adherend (in Sec. I), a bonded overlap section (in Sec. II), and an inner unbonded doubler part (in Sec. III). In the following analysis, the joint deflection and bending stiffness in each joint section can be distinguished by their subscripts. For instance, D_i is the bending stiffness in the section i ($i = 1$ to 3). Note that E_1, E_2, t_1, and t_2 refer to the Young's modulus and thickness in the adherend (subscript $i = 1$) and the doubler (subscript $i = 2$). Deflections in the unbonded adherend, overlap section, and inner doubler section for the butt joint [8,18] are given by Eqs. (4a–4c), with the origin of the coordinate frame located at the left side of each section's centroid:

$$w_1 = A_1 \cosh(\mu_1 x_1) + B_1 \sinh(\mu_1 x_1); \qquad (0 \le x_1 \le L) \tag{4a}$$

$$w_2 = A_2 \cosh(\mu_2 x_2) + B_2 \sinh(\mu_2 x_2) + \delta_1; \qquad (0 \le x_2 \le 2c) \tag{4b}$$

$$w_3 = A_3 \cosh(\mu_3 x_3) + B_3 \sinh(\mu_3 x_3) + \delta_2; \qquad (0 \le x_3 \le L_0) \tag{4c}$$

where μ_i ($i = 1$ to 3) is given by Eq. (4d), A_i and B_i ($i = 1$ to 3) are the integral constants, and x_i is the joint longitudinal position in section i measured from the origin using its coordination system (Fig. 1). The bending stiffnesses D_1, D_2, and D_3 are given by Eqs. (4e–4g), respectively, as follows:

$$\mu_i = \sqrt{\frac{T}{D_i}}; \qquad (i = 1 \text{ to } 3) \tag{4d}$$

Outer adherend section:

$$D_1 = \frac{1}{(k_{22})_{\text{adherend}}} \tag{4e}$$

Overlap section:

$$D_2 \approx D_1 + E_1 t_1 \delta_1^2 + D_3 + E_2 t_2 (\delta_2 - \delta_1)^2 \tag{4f}$$

Doubler within the inner gap section:

$$D_3 = \frac{1}{(k_{22})_{\text{doubler}}} \tag{4g}$$

For aircraft structures, the adhesive thickness is very small and should generally be within 0.12 to 0.39 mm, as suggested by [18]. The Young's modulus of the adhesive is also much less than that of the laminated adherend and doubler. Thus, the adhesive can be treated as a sort of spacer in the overlap bending stiffness calculation [Eq. (4f)], having little other effect on the overall stiffness.

The following six displacement boundary conditions are then applied:

$$w_1(x_1)|_{x_1=0} = 0, \qquad w_1(x_1)|_{x_1=L} \approx w_2(x_2)|_{x_2=0},$$
$$\left.\frac{\mathrm{d}w_1(x_1)}{\mathrm{d}x_1}\right|_{x_1=L} \approx \left.\frac{\mathrm{d}w_2(x_2)}{\mathrm{d}x_2}\right|_{x_2=0} \tag{4h}$$

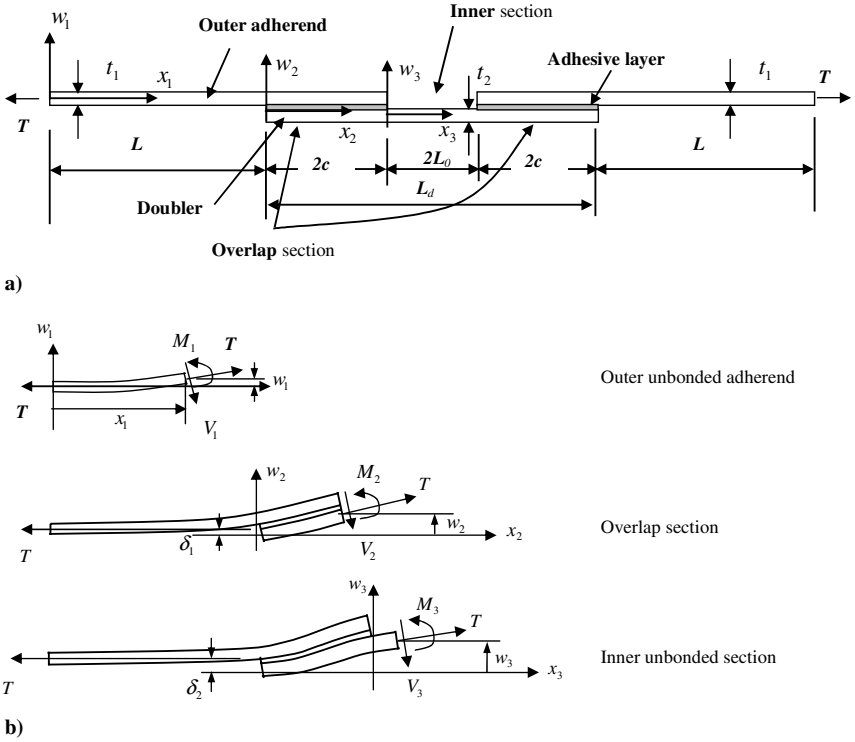

Fig. 1 Schematic diagram of a general bonded composite butt joint configuration: a) bending deformation and b) when the joint is loaded in tension (not to scale).

$$w_2(x_2)|_{x_2=2c} \approx w_3(x_3)|_{x_3=0}, \qquad \left.\frac{\mathrm{d}w_2(x_2)}{\mathrm{d}x_2}\right|_{x_2=2c} \approx \left.\frac{\mathrm{d}w_3(x_3)}{\mathrm{d}x_3}\right|_{x_3=0},$$
$$\left.\frac{\mathrm{d}w_3(x_3)}{\mathrm{d}x_3}\right|_{x_3=L_0} = 0 \tag{4i}$$

The corresponding integration constants then become

$$A_1 = 0 \tag{4j}$$

Thus, δ_1 and δ_2 can be expressed in Eqs. (4p) and (4q) as

$$\delta_1 = \frac{t_1 + t_2 + 2\eta}{2[1 + (E_1' t_1 / E_2' t_2)]} = \frac{t_1 + t_2 + 2\eta}{2[1 + (k_{11})_{\text{doubler}}/(k_{11})_{\text{adherend}}]} \tag{4p}$$

$$\delta_2 = \frac{t_1 + t_2 + 2\eta}{2} \tag{4q}$$

where η is the adhesive thickness.

The bending moments in the unbonded outer adherend, bonded overlap, and the inner doubler sections can then be expressed as

$$B_1 = \frac{\delta_1[(\mu_2/\mu_1)\tanh(2\mu_2 c) + (\mu_3/\mu_1)\tanh(\mu_3 L_0)] + (\mu_3/\mu_1)[\tanh(\mu_3 L_0)/\cosh(2\mu_2 c)](\delta_2 - \delta_1)}{\cosh(\mu_1 L)(1 + (\mu_2/\mu_1)\tanh(\mu_1 L)\tanh(2\mu_2 c) + \mu_3 \tanh(\mu_3 L_0)\{[\tanh(\mu_1 L)/\mu_1] + [\tanh(2\mu_2 c)/\mu_2]\}} \tag{4k}$$

$$A_2 = B_1 \sinh(\mu_1 L) - \delta_1 = \frac{(\mu_3/\mu_1)\tanh(\mu_1 L)\tanh(\mu_3 L_0)\{(\delta_2 - \delta_1)/[\cosh(2\mu_2 c)]\} - \delta_1[1 + (\mu_3/\mu_2)\tanh(2\mu_2 c)\tanh(\mu_3 L_0)]}{1 + (\mu_2/\mu_1)\tanh(\mu_1 L)\tanh(2\mu_2 c) + \mu_3 \tanh(\mu_3 L_0)\{[\tanh(\mu_1 L)]/\mu_1 + [\tanh(2\mu_2 c)]/\mu_2\}} \tag{4l}$$

$$B_2 = \frac{\mu_1}{\mu_2} B_1 \cosh(\mu_1 L) = \frac{(\mu_3/\mu_1)\tanh(\mu_3 L_0)\{(\delta_2 - \delta_1)/[\cosh(2\mu_2 c)]\} + \delta_1[\tanh(2\mu_2 c) + (\mu_3/\mu_2)\tanh(\mu_3 L_0)]}{1 + (\mu_2/\mu_1)\tanh(\mu_1 L)\tanh(2\mu_2 c) + \mu_3 \tanh(\mu_3 L_0)\{[\tanh(\mu_1 L)/\mu_1] + [\tanh(2\mu_2 c)/\mu_2]\})} \tag{4m}$$

$$A_3 = A_2 \cosh(2\mu_2 c) + B_2 \sinh(2\mu_2 c) + \delta_1 - \delta_2 \tag{4n}$$

$$B_3 = -A_3 \tanh(\mu_3 L_0) \tag{4o}$$

where δ_1 is the transverse (vertical) distance between the neutral planes of the adherend (outer length of L) and the bonded overlap section (overlap length of $2c$ in one adherend side), δ_2 is the transverse distance between the neutral planes of the adherend and doubler (inner gap section length of $2L_0$) in the overlap section, the adherend thickness is t_1, and the doubler thickness is t_2 (Fig. 1).

$$M_1 = D_1 \frac{\mathrm{d}^2 w_1}{\mathrm{d}x_1^2} = T B_1 \sinh(\mu_1 x_1) \tag{4r}$$

$$M_2 = D_2 \frac{\mathrm{d}^2 w_2}{\mathrm{d}x_2^2} = T[A_2 \cosh(\mu_2 x_2) + B_2 \sinh(\mu_2 x_2)] \tag{4s}$$

$$M_3 = D_3 \frac{\mathrm{d}^2 w_3}{\mathrm{d}x_3^2} = T[A_3 \cosh(\mu_3 x_3) + B_3 \sinh(\mu_3 x_3)] \tag{4t}$$

where T is the joint unit-width tensile load.

2. Joint Elongation and Longitudinal Strain

When the joint is in tension, theoretical analysis of its axial elongation should be carried out under a plane-stress condition. Ignoring out-of-plane deflection, the total joint elongation consists of four components arising from the response at 1) the outer adherends, 2) the bonded overlap section, 3) the adhesive shear between the doubler and adherend within the overlap section, and 4) the inner central unbonded (not overlapped) doubler gap section.

The joint elongation can be approximated using the following expression:

$$\Delta l = 2\Delta l_1 + 2\Delta l_2 + \eta\frac{T}{cG_a} + \Delta l_3 \tag{5a}$$

Where G_a is the adhesive shear modulus, η is the adhesive thickness, c is the half-bonded length in one adherend side, T is the joint tensile load, the elongation in one outer unbonded adherend is

$$\Delta l_1 = \frac{TL}{E_1 t_1} \tag{5b}$$

the elongations in the one-sided overlap section are

$$\Delta l_2 = \frac{T2c}{E_{\text{overlap}} t_{\text{overlap}}} \tag{5c}$$

the effect of adhesive shear is

$$\frac{T\eta}{cG_a} \tag{5d}$$

and the elongation in the inner unoverlapped doubler section is

$$\Delta l_3 = \frac{T2L_0}{E_{\text{doubler}} t_{\text{doubler}}} \tag{5e}$$

Longitudinal strain on the joint surface consists of both axial tensile strain and bending strain. Theoretical analysis of axial strain should be carried out using an in-plane condition. According to Eqs. (1a–1c), the resultant strain at the laminate surface position can be determined as

$$\varepsilon_x = k_{11}N_x \pm k_{22}M_x\frac{t}{2} = k_{11}T \pm k_{22}M\frac{t}{2} \tag{5f}$$

where the tensile + or compressive − sign is determined by the bending condition at that specific location.

3. Adhesive Stresses in Composite Butt Joints

a. Basic Parameter in Adhesive Stress Equations. A single-strap butt joint is fabricated using two single-lap joints. The coupled adhesive stress differential equations for a butt joint are identical to that of a single-lap joint, except for the boundary conditions consisting of the bending moment and shear force at the overlap ends. Through equilibrium analysis in the bonded overlap section, the adhesive stress equations can be derived as [5,19,20]

$$\frac{\mathrm{d}^3\tau_a}{\mathrm{d}x^3} + a_1\frac{\mathrm{d}\tau_a}{\mathrm{d}x} + a_2\sigma_a = 0 \tag{6a}$$

$$\frac{\mathrm{d}^4\sigma_a}{\mathrm{d}x^4} + b_1\sigma_a + b_2\frac{\mathrm{d}\tau_a}{\mathrm{d}x} = 0 \tag{6b}$$

where a_1, a_2, b_1, and b_2 are four basic parameters that have to be determined before the exploration of the adhesive peel and shear stresses, σ_a and τ_a. Among the four parameters, a_2 and b_2 are coupling parameters between the adhesive peel and shear stresses. These coupling parameters vanish when dealing with identical materials having the same thickness for the adherends and doubler.

For a composite butt joint fabricated using different adherend and doubler laminates, the four parameters can be determined as

$$a_1 \approx -\frac{G_a}{\eta}\left(k_{11\text{-adherend}} + k_{11\text{-doubler}} + t_1 k_{12\text{-adherend}} - t_2 k_{12\text{-doubler}} + \frac{t_1^2}{4}k_{22\text{-adherend}} + \frac{t_2^2}{4}k_{22\text{-doubler}}\right) \tag{6c}$$

$$a_2 = \frac{G_a}{\eta}\left(k_{12\text{-adherend}} + k_{12\text{-doubler}} + \frac{t_1}{2}k_{22\text{-adherend}} - \frac{t_2}{2}k_{22\text{-doubler}}\right) \tag{6d}$$

$$b_1 = \frac{E_a}{\eta}(k_{22\text{-adherend}} + k_{22\text{-doubler}}) \tag{6e}$$

$$b_2 \approx -\frac{E_a}{\eta}\left(k_{12\text{-adherend}} + k_{12\text{-doubler}} + \frac{t_1}{2}k_{22\text{-adherend}} - \frac{t_2}{2}k_{22\text{-doubler}}\right) \tag{6f}$$

The equations relating the adhesive stress to the joint deformation are given in Eqs. (6g) and (6h) [5,6,9,19,20].

$$\frac{\sigma_a}{E_a} = \frac{w_u - w_d}{\eta} \tag{6g}$$

$$\frac{\tau_a}{G_a} = \frac{u_u - u_d}{\eta} \tag{6h}$$

where E_a and G_a are adhesive Young's and shear moduli, w_u and w_d are deflections in the adherend and doubler, and u_u and u_d are displacements at the adherend–adhesive and adhesive–doubler interfaces.

Under a plane-strain condition, the four parameters of a_1, a_2, b_1, and b_2 can be determined using the corresponding k_{ij} terms given in Eqs. (2b–2g).

b. First Strategy for Exploring Adhesive Stresses. The uncoupled equation for the adhesive shear stress can be obtained by eliminating the peel stress in Eq. (6a) as

$$\frac{\mathrm{d}^7\tau_a}{\mathrm{d}x^7} + a_1\frac{\mathrm{d}^5\tau_a}{\mathrm{d}x^5} + b_1\frac{\mathrm{d}^3\tau_a}{\mathrm{d}x^3} + (a_1b_1 - a_2b_2)\frac{\mathrm{d}\tau_a}{\mathrm{d}x} = 0 \tag{7a}$$

The corresponding characteristic equation becomes [9,19–23]

$$\lambda[\lambda^6 + a_1\lambda^4 + b_1\lambda^2 + (a_1b_1 - a_2b_2)] = 0 \tag{7b}$$

Once the seven roots are determined, the general solution for the adhesive stress can be established, and its seven constant integrals can be identified using the following seven boundary conditions [19]:

$$\int_{-c}^{c}\tau_a\,\mathrm{d}x = -T \tag{7c}$$

$$\left.\frac{\mathrm{d}\tau_a}{\mathrm{d}x}\right|_{x=-c} = \frac{G_a}{\eta}\left[\left(k_{11\text{-adherend}} + \frac{t_1}{2}k_{12\text{-adherend}}\right)T + \left(k_{12\text{-adherend}} + \frac{t_1}{2}k_{12\text{-adherend}}\right)M_0\right] \tag{7d}$$

$$\left.\frac{\mathrm{d}\tau_a}{\mathrm{d}x}\right|_{x=c} = \frac{G_a}{\eta}\left[\left(-k_{11\text{-doubler}} + \frac{t_2}{2}k_{12\text{-doubler}}\right)T + \left(-k_{12\text{-doubler}} + \frac{t_2}{2}k_{12\text{-doubler}}\right)M_1\right] \tag{7e}$$

$$\frac{\mathrm{d}^2\tau_a}{\mathrm{d}x^2} + a_1\tau_a|_{x=-c} = \frac{G_a}{\eta}\left(k_{12\text{-adherend}} + \frac{t_1}{2}k_{22\text{-adherend}}\right)V_0 \tag{7f}$$

$$\frac{\mathrm{d}^2\tau_a}{\mathrm{d}x^2} + a_1\tau_a|_{x=c} = \frac{G_a}{\eta}\left(-k_{12\text{-doubler}} + \frac{t_2}{2}k_{22\text{-doubler}}\right)V_1 \tag{7g}$$

$$\frac{\mathrm{d}^5\tau_a}{\mathrm{d}x^5} + a_1\frac{\mathrm{d}^3\tau_a}{\mathrm{d}x^3}\bigg|_{x=-c} = -a_2\frac{E_a}{\eta}(k_{12\text{-adherend}}T + k_{22\text{-adherend}}M_0) \tag{7h}$$

$$\frac{\mathrm{d}^5\tau_a}{\mathrm{d}x^5} + a_1\frac{\mathrm{d}^3\tau_a}{\mathrm{d}x^3}\bigg|_{x=c} = a_2\frac{E_a}{\eta}(k_{12\text{-doubler}}T + k_{22\text{-doubler}}M_1) \tag{7i}$$

where M_0 and V_0 are the bending moment and shear force at the outer overlap end on adherend, while M_1 and V_1 are the bending moment and shear force at the inner overlap end on the doubler.

The general solution of the adhesive peel stress can then be explored using its fundamental equation:

$$\frac{\mathrm{d}^4\sigma_a}{\mathrm{d}x^4} + b_1\sigma_a = -b_2\frac{\mathrm{d}\tau_a}{\mathrm{d}x} \tag{7j}$$

This nonhomogeneous equation can be investigated using the variation of constants or Lagrange's method [21–23]. The general solution is established by combining the general solution of its homogeneous equation and any one particular solution of its nonhomogeneous equation. This strategy was successfully undertaken and a detailed derivation of adhesive stresses in a bonded isotropic butt joint was presented by Li [19], where the general adhesive stress solutions were determined and good agreement was shown between closed-form solutions and finite element (FE) predictions.

c. Second Strategy for Exploring Adhesive Stresses. The uncoupled sixth-order differential equation [20] for adhesive peel stress can be derived by eliminating adhesive shear stress in Eq. (6b) as

$$\frac{\mathrm{d}^6\sigma_a}{\mathrm{d}x^6} + a_1\frac{\mathrm{d}4\sigma_a}{\mathrm{d}x^4} + b_1\frac{\mathrm{d}^2\sigma_a}{\mathrm{d}x^2} + (a_1b_1 - a_2b_2)\sigma_a = 0 \tag{7k}$$

Note from the two uncoupled adhesive stress differential Eqs. (7a) and (7k) that their characteristic equations would have up to six common roots, γ_i ($i = 1$ to 6). One more characteristic root of $\lambda = 0$ exists for the adhesive shear stress. The expression for the general solution of the adhesive shear stress will have seven terms, and the expression for the general solution for the peel stress will have six terms. These six terms are identical to the adhesive shear stress expression and are determined by the characteristic roots. The second strategy would avoid the complex derivations and long expressions required for determining the adhesive peel stress used in the first strategy. Note that the final closed-form solutions for adhesive shear and peel stresses were not provided by Bigwood and Crocombe [20]. Furthermore, they did not present the six boundary conditions needed to explore the peel stress.

The same procedure used to explore the adhesive shear stress solution in the first strategy can be used in the second strategy. The seven boundary conditions were presented in [20]. Two different boundary conditions exist between the two sets of boundary conditions {Eqs. (7c–7h), (7h), and (7i) and the second set of boundary conditions in [20]}. The last two boundary conditions in [20] were replaced by the fourth and fifth conditions (Eqs. (7f) and (7g)] in the first set of boundary conditions [19]. The first boundary condition set expressed in this paper, Eqs. (7c–7h), (7h), and (7i) will be used for shear stress derivation for the bonded composite butt joints discussed herein. These boundary conditions led to good agreement between the closed-form solutions of the proposed first strategy and FE results for the butt joints made of isotropic materials [19]. Thus, the impact of the two different sets of boundary conditions on the adhesive shear stress will not be studied further.

The six integral constants in the general peel stress solution expression may be determined using the following boundary conditions:

$$\int_{-c}^{c}\sigma_a\,\mathrm{d}x = V_u|_{x=-c} - V_u|_{x=c} = V_0 \tag{7l}$$

$$\int_{-c}^{c}\sigma_a x\,\mathrm{d}x = -(V_0c + M_0) \tag{7m}$$

$$\frac{\mathrm{d}^2\sigma_a}{\mathrm{d}x^2}\bigg|_{x=-c} = \frac{E_a}{\eta}(k_{12\text{-adherend}}T + k_{22\text{-adherend}}M_0) \tag{7n}$$

$$\frac{\mathrm{d}^2\sigma_a}{\mathrm{d}x^2}\bigg|_{x=c} = -\frac{E_a}{\eta}(k_{12\text{-doubler}}T + k_{22\text{-doubler}}M_1) \tag{7o}$$

$$\frac{\mathrm{d}^3\sigma_a}{\mathrm{d}x^3} + b_2\tau_a|_{x=-c} = \frac{E_a}{\eta}k_{22\text{-adherend}}V_0 \tag{7p}$$

$$\frac{\mathrm{d}^3\sigma_a}{\mathrm{d}x^3} + b_2\tau_a|_{x=c} = -\frac{E_a}{\eta}k_{22\text{-doubler}}V_1 \tag{7q}$$

Exploration of closed-form solutions will be carried out and presented in another paper.

III. Experimental Testing Cases

A. Joints and Strain Measurement

A total of four strain-gauged joints were tested to enable comparison between theoretical, FE, and experimental results: two case 1 joints, where the adherends and doublers were the same thickness, and two case 2 joints, where the doublers were 50% thicker than the adherends. Carbon-fiber laminates were laid up using an AFP machine and then cured in an autoclave. The layup sequence for all joint adherends was $[45/-45/0/90]_{2s}$. The measured nominal thickness of this 16-layer laminate was 2.24 mm. The butt joints were assembled and cured at the panel level, then they were cut into coupons with a width of 25.4 mm. The doubler layup sequence was $[45/-45/0/90]_{2s}$ for case 1 joints and $[45/-45/0/90]_{3s}$ for case 2 joints. The thicker doubler using the 24-layer laminate was 3.36 mm in thickness. The material properties for the lamina of CYCOM 5276-1 T40-800 145/35 (Cytec Engineered Materials) used in this work were as follows: $E_{11} = 145$ GPa, $E_{22} = 8.9$ GPa, $v_{12} = 0.31$, and $G_{12} = 4.5GPa$ (these data were derived from tests on laminated sheet coupons conducted as part of this work).

The final joint dimensions and strain gauge arrangements are shown in Fig. 2. The inner gap between the two adherends was approximately 0.5 mm, and the adhesive layer thickness was approximately 0.17 mm. An elastic modulus of $E_a = 3$ GPa and a Poisson's ratio of $v_a = 0.32$ were assumed for the FM300 film adhesive, based on literature data for similar adhesives. Tapered end tabs made from a 3.18-mm-thick FR4 fiberglass sheet were bonded to the coupons using Hysol EA9396 room-temperature cure paste-type adhesive. Three strain gauges (CEA-06-062UW-350, Measurements Group, Inc., North Carolina) with a gauge factor of $2.13 \pm 0.5\%$ were mounted on each joint in the longitudinal direction. Strain gauge 1 was used to detect the strains at the center area of the doubler outer surface. Strain gauges 2 and 3 were at the same longitudinal position (7.8 mm from the overlap end), with one installed on the upper surface and the other installed on the lower surface of the same outer adherend. Bending information near the overlap end can be estimated using the strain difference between strain gauges 2 and 3.

B. Loading Condition

The adhesively bonded composite butt joints were loaded in tension using an MTS load frame equipped with a 22.5 kN load cell (model number 5631 and serial number 611.21A-01) calibrated to national standards. Tensile load was applied at a rate of 2 kN/ min up to a maximum load of 5.5 kN, after which point the specimens were

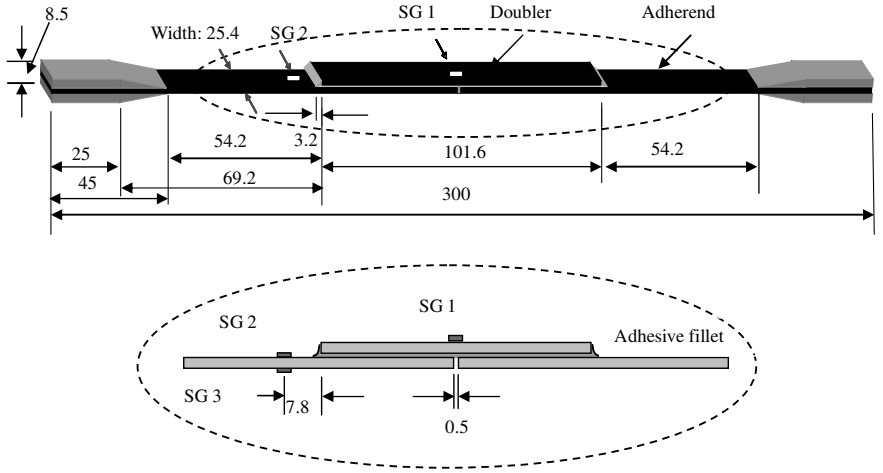

Fig. 2 The bonded composite single-strap butt joint specimen design and three strain gauge (SG) positions (all dimensions in mm).

unloaded. The joints were loaded and unloaded in this manner a total of three times. The maximum load corresponded to a remote tensile stress of approximately 97 MPa, well within the elastic range for the adherend and doubler. A linear elastic response was also assumed for the adhesive in order to simplify the subsequent theoretical analyses, an approach widely used by a number of researchers [5–8]. Notwithstanding the well-known associated compliance issues, joint elongation between the two cross heads was used to assess joint deformation, since a displacement measurement device, such as a linear variable displacement transducer that could cover the entire overlap section, was not available.

IV. Geometrically Nonlinear Finite Element Simulations

To properly set up the lamina orientation in each ply and achieve fast and accurate numerical analyses, three-dimensional FE models of the experimental joints (with unit width; i.e., 1 mm in the y direction) were generated using MSC.Patran (preprocessor and postprocessor) version 2008r2 and MSC.Marc (solver) version 2008. A total of 5330 nodes and 2536 eight-node brick elements (two wedge elements included) were used for the case 1 joint (Fig. 3), and a total of 6370 nodes and 3054 eight-node brick elements (two wedge elements included) were used for the case 2 joint (Fig. 4). The outer

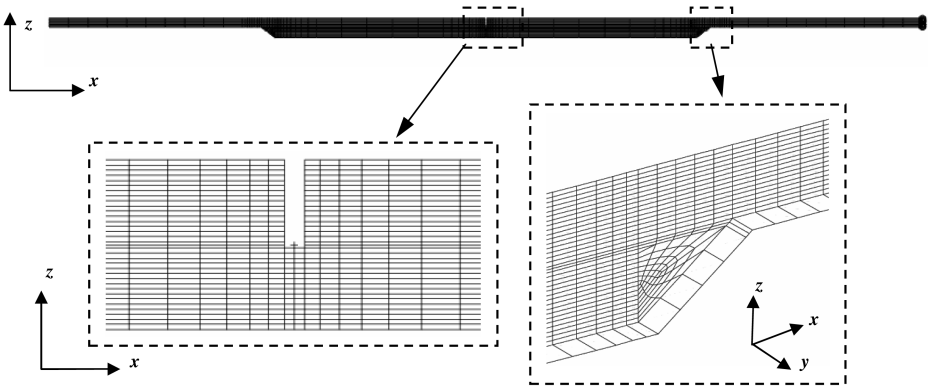

Fig. 3 The three-dimensional FE model for the case 1 joint using a total of 5330 nodes and 2536 eight-node brick elements (two wedge elements included).

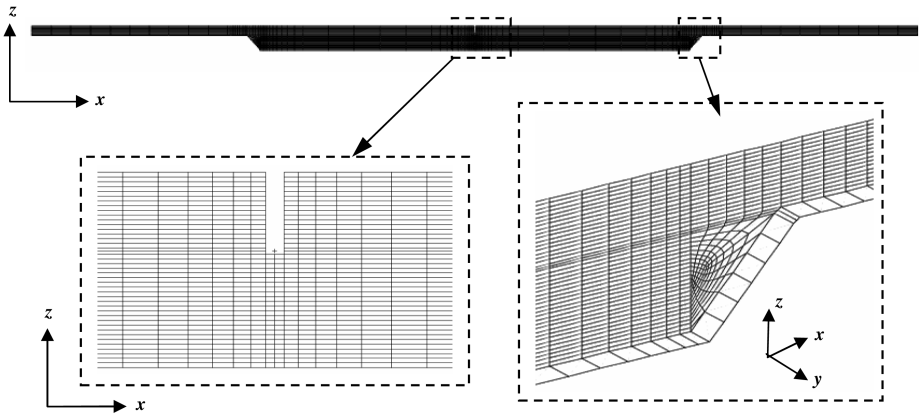

Fig. 4 The three-dimensional FE model for the case 2 joint (50% thicker doubler) using a total of 6370 nodes and 3054 eight-node brick elements (two wedge elements included).

adherend length was 54.2 mm in the models. Joint deformation under a two-dimensional plane-strain condition was analyzed by applying the zero displacement condition, $U_y = 0$, at the two joint side edges along the longitudinal x direction. The joint width direction was in the y axis, and thickness was in the z direction. One element was meshed along the joint unit width, as well as in each lamina in the thickness direction. Two elements were created along the adhesive thickness in the overlap section. A relatively fine mesh was created in the joint transition areas in the outer and inner overlap edge regions. Adhesive fillets were simply assumed to be a triangular prism at the outer overlap edges. A 0.5 mm inner gap between the two adherends, as well as the adhesive layer, was built in the models to reflect the actual joint configuration, including an adhesive crack which was induced during the first tensile ramp.

In addition to the displacement condition of $U_y = 0$ at the joint's two side edges, the following boundary conditions were used during the joint tensile loading stage: 1) displacement of $U_x = U_y = U_z = 0$ set at the joint left remote adherend edge; 2) displacement of $U_z = 0$ applied to the two middle nodes at the right remote adherend edge; 3) multipoint constraint condition applied to the nodes at the right remote edges, ensuring the same longitudinal displacement (U_x); 4) uniform tensile stress applied to the joint right adherend edge; and 5) geometrically nonlinear FEA. FEA results for each pair of nodes, located at the $[x \quad 0 \quad z]$ and $[x \quad 1 \quad z]$ positions on the two width-side surfaces, were almost identical.

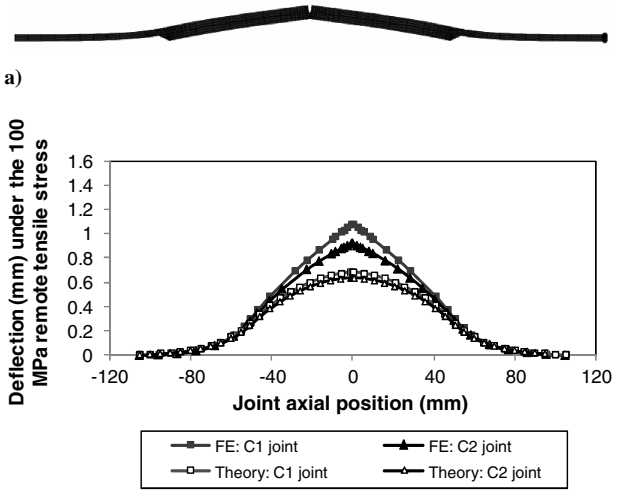

Fig. 5 Typical joint deformations: a) illustrating secondary bending in a bonded butt joint and b) comparing joint deflection predictions obtained from the FE model and the theoretical model under a 100 MPa remote tensile stress.

V. Results and Discussion

The adhesive bond within the joint middle inner gap cracked at a tensile load of approximately 4.5 kN (177 N/mm per unit width) during the first load cycle to peak load (i.e., 5.5 kN). The onset of cracking could be detected audibly as well as through a discontinuity in the measured strain curves. Strain and displacement (elongation) data from the two subsequent load cycles were used to study joint deformation. Limited differences in the elongation and strains within each joint case during the last two load ramps were found. Average data obtained from the two tests for each case 1 joint and case 2 joint were used in the following studies of the joint elongation and strain.

A. Out-of-Plane Deflection of Joint

Out-of-plane deflections (i.e., secondary bending) arise when the butt joint is in tension. Figure 5 shows joint deflections under a 100 MPa remote tensile stress, obtained from FE and theoretical results. Peak deflection occurred in the joint middle region, with a maximum magnitude of approximately 1 mm, a very small value compared with the joint overall length of the approximate 210 mm. Peak deflections were $U_z = 1.08$ mm (case 1 joint by FE), 0.90 mm (case 2 joint by FE), 0.69 mm (case 1 joint by theory under a plane-strain condition), and 0.62 mm (case 2 joint by theory under a plane-strain condition). The relative difference between theory and FE predictions was approximately 36% for the case 1 joint and 31% for the case 2 joint. This difference was mainly the result of the displacement continuity conditions constrained at the overlap edges [presented in Eqs. (4h) and (4i)] in the theoretical derivation. At the two outer overlap edges ($x = \pm 50.8$ mm positions if $x = 0$ is at the joint middle position), there was limited difference between the FE and theoretical results. FE results are more accurate than theoretical predictions, since approximate displacement boundary conditions were used at the joint transition edges in the theoretical derivations. It can be seen from Fig. 5 that 1) the theoretical model underestimated the deflection at the inner overlap edge region; and 2) the deflection difference was lower for the thicker doubler. As a result, the bending moment would be overestimated at the inner overlap edge and underestimated at the middle position of inner gap region. The impact of these shortfalls on the joint strain could be partially discerned in the subsequent strain comparisons. In general, the theoretical model was found to correlate well with the FE results within the applied load range.

B. Joint Elongation

Joint elongation versus tensile load is shown in Fig. 6. A linear variation was observed, and good agreement was found between experimental, theoretical, and FE results. For the current elongation estimation using Eq. (5a), the value of the outer unbonded adherend length used was $L = 69.2$ mm. This length was measured from the tabbed edge of the gripped part to the adherend bonded overlap edge,

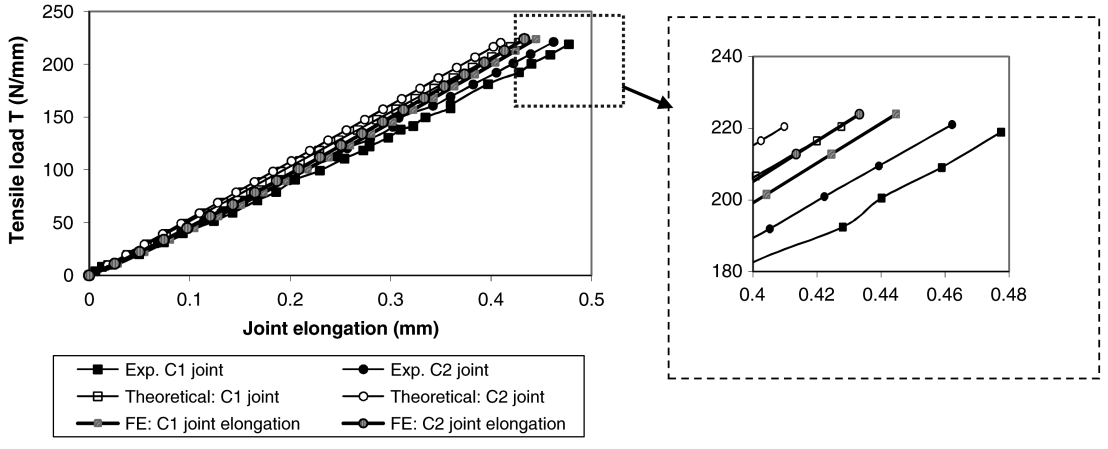

Fig. 6 Comparison of the joint elongation during the tensile loading stage obtained from the experimental tests and theoretical estimations.

as shown in Fig. 2. Since the stiffnesses of both the adhesive fillets and the tapered tabs are very low, their contributions to the overall joint stiffness can safely be ignored. Theoretical joint elongation results were obtained using Eq. (5a). As stated earlier, identical laminated adherends were used in both joint cases. The only difference between the two was the doubler that, for the case 2 joint, was 50% thicker than the case 1 joint; for the case 1 joint, the doubler was identical to the adherends. At the peak tensile force of 220 N/mm, theoretically predicted joint elongations were approximately 90 and 89% of the measured values for the case 1 and case 2 joints, respectively, with the FE results falling between measured and theoretical values. The overprediction of joint stiffness may be the result of several factors: 1) inaccuracy in the elongation estimated for the overlap section and its transition area; 2) differences between the effective laminate Young's moduli used in the theoretical model and the FE models, and those in the actual tests; 3) possible slip between the grips and the joint end tabs; 4) impact of adhesive shear deformation between the end tab and joint adherend; and 5) differences in dimensions of the designed and manufactured/tested joints, etc. Despite these factors, the theoretical model correlated quite well with the experimental and FE results.

C. Strain Variation at the Longitudinal Strain Gauges

1. Effect of Plane-Strain and Plane-Stress Conditions on Axial Strains

Joint strain measurements could be used to determine if it is more appropriate for the theoretical model to use plane-strain or plane-stress assumptions. Axial strain in the inner gap section can be easily estimated using either the measured strain from gauges 2 and 3 at the outer adherend or strain results ε_x^0 from the theoretical analysis [Eqs. (2e) and (3c)]. For the case 1 joint, the axial strain in the inner gap section should be the same as that for the outer adherend. For the case 2 joint, the axial strain in the inner gap section should be $t_1/t_2 \approx 0.67$ of the outer adherend axial strain, due to the 50% thicker doubler.

Since strain gauge 1 measured the resultant strain from deformation in three areas, including the overlap end regions, this gauge could not be used to estimate axial strain for the inner section. The average of the strains measured by gauges 2 and 3 were used to determine the axial strain of the outer adherend using

$$\varepsilon_{\text{axial}} = \frac{\varepsilon_{G2} + \varepsilon_{G3}}{2} \tag{8a}$$

The corresponding axial strain was theoretically estimated using

$$\varepsilon_{\text{axial}} = \frac{T}{E_1' t_1} \tag{8b}$$

where T, t_1, and E_1' are joint tensile load (per unit width), adherend thickness, and the effective Young's modulus of the adherend laminate, respectively. E_1' is E_1 under the plane-stress condition, and E_1' becomes $E_1/(1 - \upsilon_{12}\upsilon_{21})$ under plane-strain conditions. Figure 7 shows the axial strain variation in the outer adherend obtained from experimental, theoretical, and FE results. For the two joint cases, axial strains in the outer adherend should be the same since they used identical adherends. In both cases, the best agreement was achieved between the experimental data and theoretical results under an assumed plane-stress condition. In particular, experimental data in the case 1 joint were virtually identical to the theoretical results. The theoretically predicted strains under plane-strain conditions were approximately 8% lower for the case 1 joint and 10% for the case 2 joint. The FE results were between the theoretical results under plane-stress and plane-strain conditions. This suggests that a plane-stress condition provides a closer estimation of joint axial strains and validated the later use of a plane-stress condition for joint elongation analysis. As predicted, the stiffer doubler of the case 2 joint did not significantly affect the longitudinal strain in the adherends. Two samples for each joint case were tested with a measured difference of no greater than 2.5% for any reading.

2. Strain Analysis Approach in Strain Gauge 1 for Theoretical Model

Strain gauges 2 and 3 had an effective gauge length of approximately 1.58 mm, which spanned only one section of the adherend, well away from the overlap ends. Thus, constant strain within the gauge length could be assumed: i.e., no strain gradient. Theoretical estimations for these strains can be obtained using Eq. (5f).

On the other hand, strain gauge 1 spanned three different sections, as shown in Figs. 2 and 8a: a 0.54 mm length on the left-side overlap section, a 0.5 mm length on the inner gap section, and a 0.54 mm length on the right-side overlap section. Since the strain variation along the doubler outer surface should be continuous, an approach is proposed here to ensure strain continuity and to estimate the corresponding average strain. This approach aims to provide a useful application of the theoretical analysis method, as well as to provide an explanation of the obtained experimental data. The left- and right-side overlap sections had the same deformation and strain variation. Since there could be little strain variation within each of the three small sections, a constant distribution was assumed to exist in each section. Three points, A, B, and C, were chosen at the left edge, center, and right edge of the strain gauge, such that they were away from the overlap end. The strain at point A was the same as the strain at point C. According to the mode of joint deformation, the strain at point B was compressive with a strain magnitude greater than at points A and C. Strains at these points, estimated using Eq. (5f), were assumed to be constant throughout each section. As shown in Figs. 8b and 8c, two different strain discontinuity scenarios were encountered through application of a tensile load to the joints; these can be dealt with using the following approaches.

a. Strain Situation 1. When the strain ε_A at both points A and C was positive (in tension) and the strain ε_B at point B was in compression, the assumed linear strain variation is shown in the right side of Fig. 8b. The algebraic sum in these positive and negative areas was computed and the average strain was determined by direct

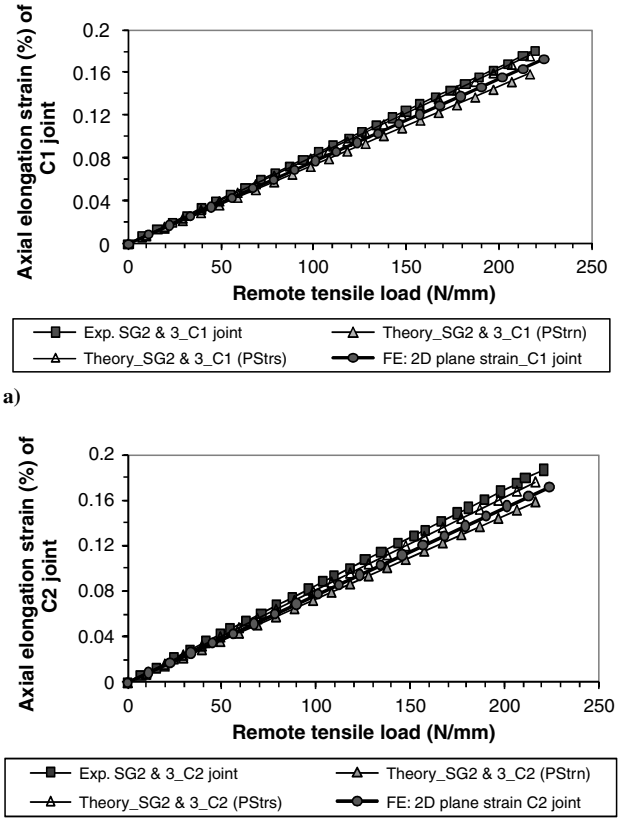

Fig. 7 Comparison of experimental and theoretical adherend axial strains at strain gauge 2 and 3 positions for a) C1 (case 1) and b) C2 (case 2) joints. PStrn and PStrs refer to the plane-strain and plane-stress conditions, SG refers to strain gauge, and 2D denotes two-dimensional.

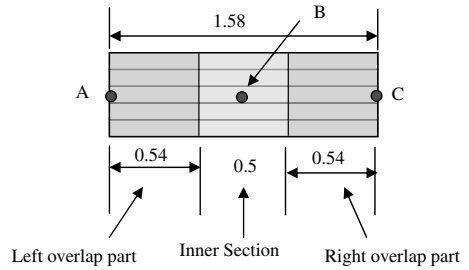

a) Three regions covered by the 1.58 mm gauge length of strain gauge 1

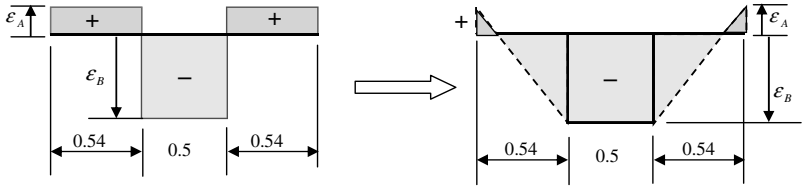

b) Strain situation 1 and its continuity approach

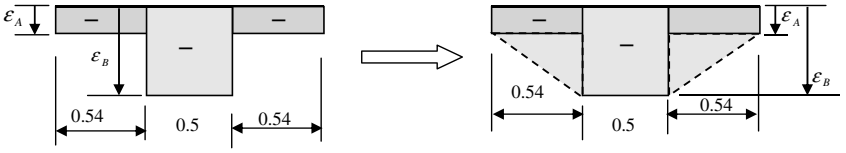

c) Strain situation 2 and its continuity approach

Fig. 8 Schematic of the approximate approach used to ensure strain continuity within the gauge length of strain gauge 1 for two different strain distribution scenarios (dimensions in mm).

summation of the strain areas and dividing by the 1.58 mm gauge length.

b. Strain Situation 2. When the strains at points A (or C) and B were negative (in compression), the assumed linear strain variation is shown in the right side of Fig. 8c. The average strain was again computed by summing the strain areas and dividing by the 1.58 mm gauge length.

The two situations can be easily identified during tensile loading. An Excel spreadsheet was then used to compute the corresponding average strain for comparison with the experimental data.

3. Strain Comparison

Longitudinal strain was calculated under both plane-strain and plane-stress conditions. This was accomplished using Eq. (5f) with the appropriate Young's modulus and bending stiffness. The joint bending moments [second term in Eq. (5f)] can be calculated using Eqs. (4r–4t) for specific locations. The related six integral constants [Eqs. (4j–4o)] can be determined using the corresponding joint geometric data ($L = 54.2$ mm, $2c = 50.55$ mm, $L_0 = 0.25$ mm, etc.) and remote tensile load. If a value of $L = 69.2$ mm is used, the calculated bending moments at the outer overlap end are almost identical to those ones obtained using a value of 54.2 mm, since the effect of the adherend length on the bending moment variation at the outer overlap end region can be eliminated for joints when $L/c > 2$ [8].

FE results were taken from the nodes corresponding to strain gauges 2 and 3, while average strain from the nodes located within the strain gauge region was used to represent the strain gauge 1 value due to the large local strain variations.

Figure 9 shows the longitudinal strains obtained from the three methods for the case 1 (Fig. 9a) and case 2 (Fig. 9b) joints. This strain consisted of the axial strain component under a plane-stress condition and the strain induced by bending. Good agreement was achieved among experimental, theoretical, and FE results in both joints, especially for the case 1 joint. In both cases, FE results were virtually identical to experimental data at the three strain gauge locations. Similar strain variations were observed in the two joint cases, with compressive strain occurring at strain gauge 1 and tensile

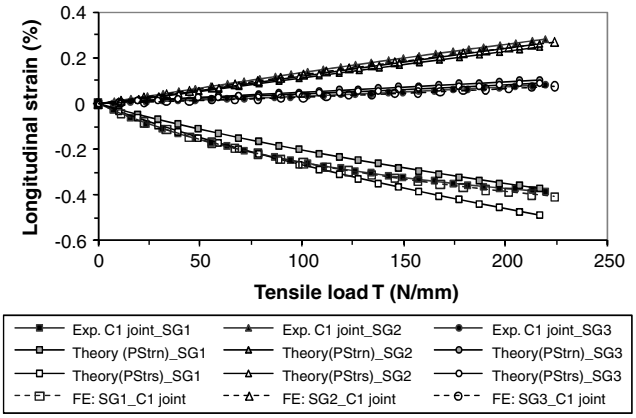

a) Case 1 joint (C1 joint) using identical laminates

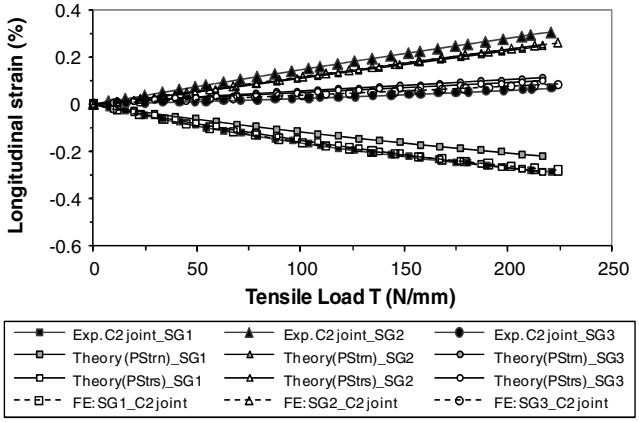

b) Case 2 joint (C2 joint) with thicker doubler

Fig. 9 Comparisons of longitudinal strains of strain gauges 1 to 3 for the two joint cases obtained from experimental measurements and theoretical calculations.

Table 1 Strains in strain gauges 2 and 3 obtained from experimental measurement and theoretical analysis at a tensile load of 220 N/mm (unit width), referring to Fig. 9

Condition	Case 1 joint			Case 2 joint		
	Strain gauge 2 (SG 2)	Strain gauge 3 (SG 3)	Difference (ε_{SG2}-ε_{SG3})	Strain gauge 2	Strain gauge 3	Difference (ε_{SG2}-ε_{SG3})
Experimental and FE strain	0.27%	0.07%	0.20%	0.29%	0.08%	0.21%
Theoretical (plane stress) strain	0.25%	0.092%	0.16%	0.25%	0.11%	0.14%
Theoretical (plane strain) strain	0.26%	0.11%	0.15%	0.24%	0.11%	0.13%

strains occurring at strain gauges 2 and 3. The stiffer doubler in the case 2 joint led to markedly smaller strains in the inner section (strain gauge 1) than in the case 1 joint, which also affected the strains at the outer adherends. The measured strains at strain gauges 1, 2, and 3 in the case 1 joint were approximately 135, 92, and 118%, respectively, higher than the corresponding strains in the case 2 joint. Additional details regarding each strain gauge response are given next.

a. Strain Gauge 1. For the case 1 joint (Fig. 9a), the measured strains and FE results were between the strains estimated assuming plane-strain and plane-stress conditions, with strains predicted using a plane-stress condition being slightly greater than those predicted using a plane-strain condition. The strain difference between these two predictions was approximately 0.11% at peak load (220 N/mm tensile load). For a tensile load from 0 to 100 N/mm, the measured strains could be accurately predicted using a plane-stress assumption; for tensile loads between 100 and 175 N/mm, the measured strains were between those calculated using plane-strain and plane-stress conditions; and for a tensile load between 175 to 220 N/mm, the measured strains compared better with those estimated using a plane-strain assumption.

For the case 2 joint (Fig. 9b), the measured strain gauge 1 strains were best represented assuming a plane-stress condition during the entire tensile loading ramp. The FE results were virtually identical to the measured data. The difference between these two predictions (plane stress and plane strain) was less than that of case 1 joint, with a maximum difference of 0.066% at the highest tensile load of 220 N/mm. The excellent agreement between the experimental, FE, and theoretical results for strain gauge 1 demonstrated that the approach proposed for ensuring strain continuity and for estimating the average strain is acceptable as a practical engineering solution.

b. Strain Gauges 2 and 3. The maximum strain difference between the plane-stress and plane-strain conditions at each strain gauge location was approximately 0.013% at the 220 N/mm tensile load for both joints, much less than the differences in strain gauge 1. This strain difference may be affected by the degree of bending in the joint; the larger the degree of bending, and the greater the strain difference.

The theoretical predictions matched the experimental results for both the case 1 and case 2 joints. Table 1 gives both experimental and theoretical strains when these joints were loaded at the maximum tensile load of 220 N/mm. From the measured strain data (ε_{SG2}-ε_{SG3}), it can be seen that the degree of outer adherend bending was slightly greater in the case 2 joint than in the case 1 joint. This difference could not be clearly seen in the theoretical calculations.

The discrepancy in the strain comparisons between the experimental, FE, and theoretical predictions could be explained by the following: 1) differences between the averaging approach used in the theoretical calculations and the actual measured strain gauge values, 2) differences in the actual and modeled material properties, and 3) inaccuracies in the idealized joint condition used in the theoretical analysis; for example, adhesive fillets at the overlap ends and the joint tapered tabs were not included, etc. [24]. In general, good agreement in strains between the theoretical, FE, and experimental results was achieved, demonstrating that the proposed approach for ensuring strain continuity in the overlap end region can be used for practical applications and that the theoretical methods for the strain analysis are not affected as significantly as the deflection prediction.

D. Adhesive Stress Profile Along Longitudinal Bondline

Derivation of a closed-form solution for adhesive stress would be a tedious job, even with several simplifications in joint configuration and material behavior [19]. For bonded composite butt joints with different adherends and doublers, no closed-form solutions were found in the open literature. FE results were used in this study. Figure 10 shows the adhesive peel stress profile indicating sharp changes at the overlap edges, especially at the inner edge. The highest peak stress was located at the inner edge and was much greater than the outer edge value due to the secondary bending condition. The

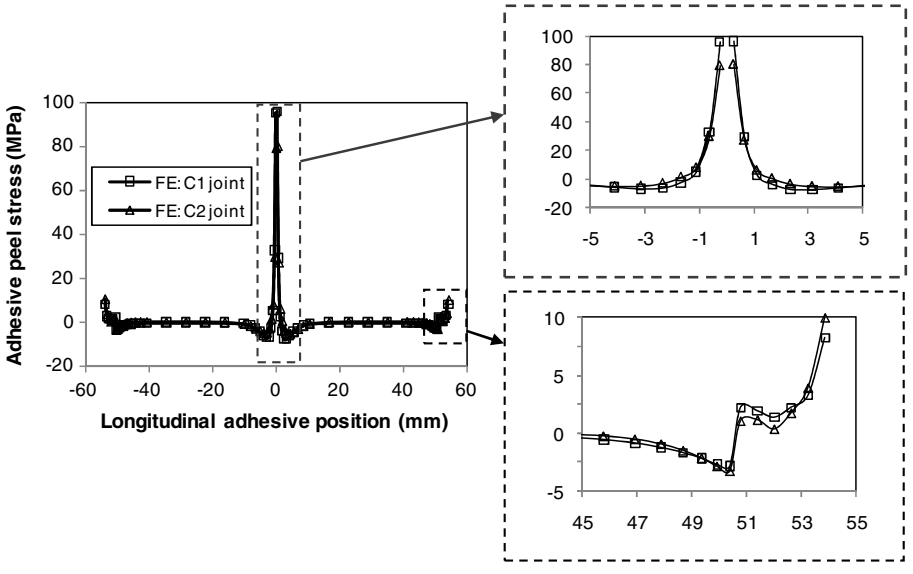

Fig. 10 Adhesive peel stress σ_a variation along the bondline for the 100 MPa joint remote tensile stress predicted by FEA.

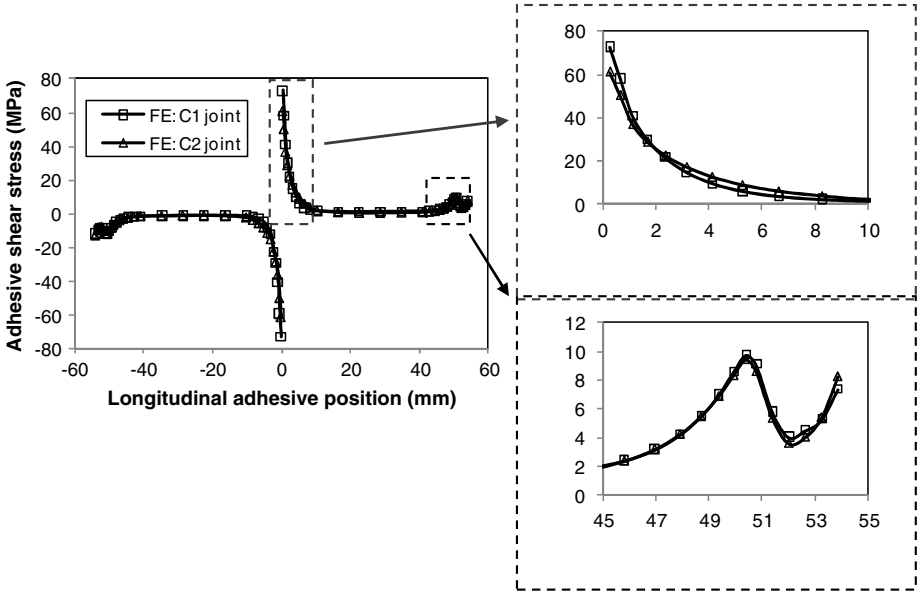

Fig. 11 Adhesive shear stress τ_a variation along the bondline for the 100 MPa joint remote tensile stress predicted by FEA.

highly nonlinear region was approximately 10 mm in length in both the outer and inner overlap edge regions, with almost zero peel stress within the overlap middle section, as shown in this figure. The peak stress at the inner overlap edge was approximate 96 MPa for the case 1 joint and 80 MPa for the case 2 joint, a difference of about 17% for the thicker doubler. The stress magnitude at the outer overlap edge was effectively decreased by the presence of an adhesive fillet, compared with a nonfillet joint case [19]. The maximum peel stress was calculated to be approximately 8 MPa in the case 1 joint and 10 MPa in the case 2 joint at the outer overlap fillet region.

The adhesive shear stress profile is shown in Fig. 11, with a similar profile to the peel stress. The highly nonlinear stress distribution was similar to the peel stress and occurred within approximately 10 mm of the outer and inner overlap edge regions. Again, near-zero shear stress was found within the overlap middle section. Peak stress was located at the inner edge and was much greater than the outer edge value at approximately 73 MPa for the case 1 joint and 60 MPa for the case 2 joint. The magnitude of the adhesive shear stress at the outer overlap edge was approximately 10 MPa for both joint cases. The strength of the bonded butt joint would be mainly affected by the adhesive stress at the inner edge region.

Because of the high peak adhesive stresses at the bonded overlap edges, especially at the inner overlap edges, overall joint integrity strength could be dramatically reduced. This joint configuration was characterized by Hart-Smith in 1985 [10] as being barely qualified as a means of transferring load because of built-in stress concentrations. Local strengthening should be undertaken at the bonded butt joint, especially at the inner overlap end area, to effectively decrease the bending deflection and the adhesive peel stress magnitude. To ensure a progressive failure mode, the introduction of mechanical fasteners could be considered to ensure a sufficient margin of safety. Thus, this butt joint configuration can be effectively accepted and used in new generation aircraft with the extensive use of composites.

VI. Conclusions

Two different adhesively bonded composite single-strap joints in tension were tested in the elastic range. A joint elongation expression was presented and was shown to be within 10% of the experimental results in all cases. Possible sources of the slightly overestimated joint stiffness were identified. The effect of using a 50% thicker doubler on joint elongation was measured experimentally, and this behavior was reflected in the developed elongation model.

To theoretically study the secondary bending of the bonded composite butt joints, effective parameters such as Young's modulus and bending stiffness were derived under both plane-strain and plane-stress conditions, allowing the further assessment of the impact of the two conditions on the joint deflection and degree of bending.

Two three-dimensional FE models were created to model the response of the two composite butt joints. A unit-width model was used in the FEA, and joint deformation under plane-strain condition was carried out using appropriate displacement conditions.

Comparing theoretical and FE results with the experimentally measured axial strains in the outer adherend, it was found that 1) the FE results lay between theoretical predictions and the experimental data, and 2) the theoretical analyses of the joint coupon elongation and axial strain should be carried out using a plane-stress assumption.

An approach was proposed to deal with the theoretical strain discontinuity in the doubler within the inner overlap end section (across the length of the strain gauge used). This strain discontinuity was an artifact of inappropriate use of the Euler–Bernoulli beam theory at the end of the overlap. Modified theoretical strains at the inner overlap end section were determined and compared with the measured strains. Good agreement between the experimental, FE, and theoretical strain results was achieved, demonstrating that Euler–Bernoulli beam theory combined with the proposed approach could be used for practical strain analysis in bonded composite butt joints in the elastic deformation range.

Variation in the theoretically predicted strains indicated that the strain induced by secondary bending under both plane-strain and plane-stress conditions should be studied at locations with high bending load, such as the overlap ends and the inner doubler gap regions, since the difference in these strains under the two conditions is significant. These conditions represent upper and lower bounds on the actual strain state.

Four coefficients of the adhesive stress equations for the composite butt joint configuration were determined, and two strategies were presented to solve these higher-order differential stress equations.

Variation in adhesive stress along the longitudinal bondline was numerically studied; FE results suggested that extra strengthening should be applied to the geometrical transition areas, especially the inner overlap edge region, in order to ensure structural integrity.

Acknowledgments

This work has been carried out under IAR Program 303 Aerospace Structures, Institute for Aerospace Research (IAR)/National Research Council Canada 2007 Project 46NS-8CTCJ, Mechanical Behaviour of Bonded/Bolted Composite-to-Composite Joints. The

financial support received from IAR is acknowledged and greatly appreciated. Our sincere acknowledgement to J. H. Chen, D. Backman, T. Benak, B. Moyes, T. Kay, M. Delannoy, and D. Alloggia for their valuable contributions to this work.

References

[1] Smith, P. A., and Pascoe, K. J., "The Effect of Stacking Sequence on the Bearing Strengths of Quasi-Isotropic Composite Laminates," *Composite Structures*, Vol. 6, Nos. 1–3, 1986, pp. 1–20. doi:10.1016/0263-8223(86)90065-6

[2] Hart-Smith, L. J., "Adhesive Bonding of Composite Structures: Progress to Date and Some Remaining Challenges," *Journal of Composites Technology and Research*, Vol. 24, No. 3, 2002, pp. 133–151. doi:10.1520/CTR10566J

[3] Xiao, Y., and Ishikawa, T., "Bearing Strength and Failure Behaviour of Bolted Composite Joints, Part I: Experimental Investigation," *Composites Science and Technology*, Vol. 65, Nos. 7–8, 2005, pp. 1022–1031. doi:10.1016/j.compscitech.2005.02.011

[4] Kweon, J. H., Jung, J. W., Kim, T. H., Choi, J. H., and Kim, D. H., "Failure of Carbon Composite-To-Aluminum Joints with Combined Mechanical Fastening Adhesive Bonding," *Composite Structures*, Vol. 75, Nos. 1–4, 2006, pp. 192–198. doi:10.1016/j.compstruct.2006.04.013

[5] Goland, M., and Reissner, E., "The Stresses in Cemented Joints," *Journal of Applied Mechanics*, Vol. 11, 1944, pp. A17–A27.

[6] Oplinger, D. W., "Effects of Adherend Deflections in Single Lap Joints," *International Journal of Solids and Structures*, Vol. 31, No. 18, 1994, pp. 2565–2587. doi:10.1016/0020-7683(94)90037-X

[7] Li, G., Lee-Sullivan, P., and Thring, R. W., "Nonlinear Finite Element Analysis of Stress and Strain Distributions Across the Adhesive Thickness in Composite Single-Lap Joints," *Composite Structures*, Vol. 46, No. 4, 1999, pp. 395–403. doi:10.1016/S0263-8223(99)00106-3

[8] Li, G., Chen, J. H., and Yanishevsky, M., "Analytical Optimization of Bonded Single-Strap Composite Joint Size for Experimental Testing," Proceedings of the 20th Aerospace Structures and Materials Symposium, Canadian Aeronautics and Space Inst., Paper 108, Kanata, Canada, 5–7 May 2009.

[9] Delale, F., Erdogan, F., and Aydinoglu, M. N., "Stresses in Adhesively Bonded Joints: A Closed-Form Solution," *Journal of Composite Materials*, Vol. 15, No. 3, 1981, pp. 249–271. doi:10.1177/002199838101500305

[10] Hart-Smith, L. J., "Designing to Minimize Peel Stresses in Adhesive-Bonded Joints," *Delamination and Debonding of Materials*, edited by W. S. Johnson, American Soc. for Testing and Materials, Rept. ASTM STP 876, Philadelphia, 1985, pp. 238–266.

[11] Tsai, M. Y., Morton, J., and Matthews, J., "Experimental and Numerical Studies of a Laminated Composite Single-Lap Adhesive Joint," *Journal of Composite Materials*, Vol. 29, No. 9, 1995, pp. 1254–1275. doi:10.1177/002199839502900906

[12] van Rijn, L. P. V. M., "Towards the Fastenerless Composite Design," *Composites, Part A: Applied Science and Manufacturing*, Vol. 27, No. 10, 1996, pp. 915–920. doi:10.1016/1359-835X(96)00009-7

[13] Li, G., Chen, J. H., Alloggia, D., Benak, T., and Yanishevsky, M., "Experimental Study of the Fatigue Crack Growth Behaviour of Bonded Composite Single-Strap Joints," Proceedings of the 20th Aerospace Structures and Materials Symposium, Canadian Aeronautics and Space Inst., Paper 109, Kanata, Canada, 5–7 May 2009.

[14] Whitney, J. M., *Structural Analysis of Laminated Anisotropic Plates*, Technomic, Lancaster, PA, 1987.

[15] Fridman, Y., and Abramovich, H., "Enhanced Structural Behaviour of Flexible Laminated Composite Beams," *Composite Structures*, Vol. 82, No. 1, 2008, pp. 140–154. doi:10.1016/j.compstruct.2007.05.007

[16] Lifshitz, J. M., and Gildin, D., "Failure of Delaminated Carbon/Epoxy Composite Beams under Cyclic Compression," *Composite Structures*, Vol. 39, Nos. 3–4, 1997, pp. 289–296. doi:10.1016/S0263-8223(97)00121-9

[17] Machado, S. P., "Geometrically Non-Linear Approximations on Stability and Free Vibration of Composite Beams," *Engineering Structures*, Vol. 29, No. 12, 2007, pp. 3567–3578. doi:10.1016/j.engstruct.2007.08.009

[18] "Structural Behavior of Joints," *MIL-HDBK-17-3F: Composite Materials Handbook*, U.S. Department of Defense, Vol. 3, Jan. 1997, Chap. 6.

[19] Li, G., "Elastic Analysis of Closed-Form Solutions for Adhesive Stress in Bonded Single-Strap Butt Joints," *Journal of Mechanics of Materials and Structures*, Vol. 5, No. 3, 2010, pp. 409–426. doi:10.2140/jomms.2010.5.409

[20] Bigwood, D. A., and Crocombe, A. D., "Elastic Analysis and Engineering Design Formulae for Bonded Joints," *International Journal of Adhesion and Adhesives*, Vol. 9, No. 4, 1989, pp. 229–242. doi:10.1016/0143-7496(89)90066-3

[21] Edition Group, *Mathematics Handbook*, published by Advanced Education Press of China, Beijing, 1979 (in Chinese).

[22] Derrick, W. R., and Grossman, S. I., *A First Course in Differential Equations with Applications*, 3rd ed., West Publishing Co., St. Paul, MN, 1987.

[23] Kreyszig, E., *Advanced Engineering Mathematics*, 7th ed., Wiley, New York, 1993.

[24] Li, G., and Lee-Sullivan, P., "Finite Element and Experimental Studies on Single-Lap Balanced Joints in Tension," *International Journal of Adhesion and Adhesives*, Vol. 21, No. 3, 2001, pp. 211–220. doi:10.1016/S0143-7496(00)00052-X